

University of New Hampshire  
**University of New Hampshire Scholars' Repository**

---

Master's Theses and Capstones

Student Scholarship

---

Winter 2007

# Nanoscale molding of bulk metallic glass

Kavic William Rason

*University of New Hampshire, Durham*

Follow this and additional works at: <https://scholars.unh.edu/thesis>

---

## Recommended Citation

Rason, Kavic William, "Nanoscale molding of bulk metallic glass" (2007). *Master's Theses and Capstones*. 343.  
<https://scholars.unh.edu/thesis/343>

This Thesis is brought to you for free and open access by the Student Scholarship at University of New Hampshire Scholars' Repository. It has been accepted for inclusion in Master's Theses and Capstones by an authorized administrator of University of New Hampshire Scholars' Repository. For more information, please contact [nicole.hentz@unh.edu](mailto:nicole.hentz@unh.edu).

# **NANOSCALE MOLDING OF BULK METALLIC GLASS**

**BY**

**KAVIC WILLIAM RASON**

**Baccalaureate of Science, Clarkson University, 2002**

**THESIS**

**Submitted to the University of New Hampshire**

**in Partial Fulfillment of**

**the Requirements for the Degree of**

**Master of Science**

**in**

**Mechanical Engineering**

**December, 2007**

UMI Number: 1449602

UMI<sup>®</sup>

---

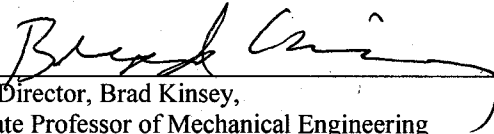
UMI Microform 1449602

Copyright 2008 by ProQuest Information and Learning Company.  
All rights reserved. This microform edition is protected against  
unauthorized copying under Title 17, United States Code.

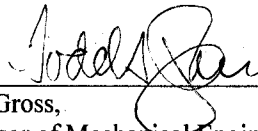
---

ProQuest Information and Learning Company  
300 North Zeeb Road  
P.O. Box 1346  
Ann Arbor, MI 48106-1346

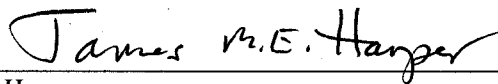
This thesis has been examined and approved



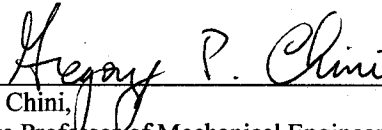
Thesis Director, Brad Kinsey,  
Associate Professor of Mechanical Engineering



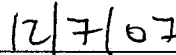
Todd Gross,  
Professor of Mechanical Engineering



James Harper,  
Professor of Physics



Gregory Chini,  
Associate Professor of Mechanical Engineering



Date

## ACKNOWLEDGEMENTS

Support from NSF (ECE #0425826) for my research is gratefully acknowledged. Also, I appreciate the assistance from Dr. Todd Gross (UNH) for Atomic Force Microscope, Dr. James Harper (UNH) for Ion Beam Deposition of Gold, and the Kostas Center for Nanomanufacturing at Northeastern University for Scanning Electron Microscopy, Electron Beam Lithography and Reactive Ion Etching,. Finally, I would like to thank Atakan Peker (LiquidMetal Technologies Inc.) for providing the Vitreloy-1b material used and performing the preliminary molding experiments.

## TABLE OF CONTENTS

ACKNOWLEDGEMENTS .....	iii
LIST OF TABLES .....	v
LIST OF FIGURES.....	vi
ABSTRACT .....	viii
CHAPTER	
1. INTRODUCTION AND BACKGROUND .....	1
2. EXPERIMENTAL INVESTIGATION .....	5
2.1 Experimental Setup .....	5
2.2 Experimental Results .....	9
2.3 Discussion.....	12
3. NANO-MOLDING THEORETICAL MODEL .....	14
3.1 Model Development .....	14
3.2 Results .....	22
3.3 Discussion .....	23
4. SQUEEZED, THIN FILM THEORETICAL MODEL .....	25
4.1 Model Development .....	25
5. CONCLUSIONS .....	33
6. FUTURE WORK .....	34
REFERENCES .....	38

## LIST OF TABLES

Table 2-1. Geometry values of low aspect ratio features created in SiO <sub>2</sub> mold without viscous flow.....	11
--	----

## LIST OF FIGURES

Figure 1-1. Schematic Temperature Time Transition (TTT) diagram illustrating rapid quench casting of a BMG from its molten state (1) and a thermoplastic molding process of the material in its supercooled liquid state (2).....	2
Figure 2-1. Schematic of experimental set-up including components for heating and cooling.....	5
Figure 2-2. Picture of the experimental set-up.....	6
Figure 2-3. (left) Approximately 340nm wide trench in SiO <sub>2</sub> and (right) approximately 300nm wide trench in SiO <sub>2</sub> following Gold deposition. ....	8
Figure 2-4. A typical trench found in Silicon mold .....	8
Figure 2-5. AFM image of a Vit-1b specimen formed into a 5mm x 5mm SiO <sub>2</sub> mold at 450°C for 2 minutes with an applied molding pressure of 100 MPa (top) and corresponding cross sectional topography for selected feature cross sections (bottom)...	10
Figure 2-6. SEM image of a Vit-1b specimen formed into a 5mm x 5mm silicon mold at 450°C for 2 minutes with an average applied molding pressure of 100 MPa. (left) Specimen Tilt is 80° providing a near cross sectional view of feature meniscus (right) alternative view demonstrating uniformity of formed features.....	12
Figure 3-1. Schematic of molding process including definitions of parameters .....	17
Figure 3-2. Recrystallization time and viscosity vs temperature for Vit-1b as documented by Schroers et al [6].....	20



Figure 3-3. Predicted filled depth for two mold trench widths and molding temperatures versus applied pressure. ....	23
Figure 4-1. Macroscopic schematic of the molding process a) initially, b) as the BMG is squeezed and flows laterally, and c) with the final thin film of BMG between the mold and the platen.....	26
Figure 4-2. Equating of average applied pressure with undefined film pressure .....	28
Figure 4-3. Predicted pressure distribution within the thin film of BMG .....	31
Figure 4-4. Schematic of material flow in the molding process.....	31
Figure 6-1. Chip pattern layout (top) and pattern detail (bottom) of nanomolding test chip to be fabricated via Deep Reactive Ion Etching.....	35
Figure 6-2. Pattern layout (left) and pattern detail (right) for chips intended for verification of thin film model.....	36

## **ABSTRACT**

### **NANOSCALE MOLDING OF BULK METALLIC GLASS**

by

**Kavic William Rason**

**University of New Hampshire, December, 2007**

Geometrically complex, high aspect ratio microstructures and limited aspect ratio nanostructures have been successfully fabricated in supercooled Bulk Metallic Glass (BMG) substrates by molding against patterned Silicon and Silicon dioxide substrates. However, demand exists for similar metallic substrates with high aspect ratio, nanoscale features. Van Der Waals based interfacial energies between the supercooled liquid BMG and the Silicon cavity may represent a substantial obstacle to the direct scaling of the molding process to the nanoscale. In an effort to investigate these effects, experiments were conducted using molds of various compositions: Silicon, SiO<sub>2</sub> and SiO<sub>2</sub> coated with Gold. The Gold coating failed to impact molding performance due to the thin layer deposited. However, drastically superior results were obtained by using a Silicon mold possibly because of the variation in interfacial interaction between the BMG and the mold material. In order to analyze the process, two theoretical models were developed. One model predicts the achievable aspect ratio of the molded features and was found to be in qualitative agreement with experimental results. The other model analyzes the BMG in the molding process as a squeezed viscous film. Finally, a value for the surface tension of Viterloy-1b within its supercooled liquid state was deduced from experimental data.

## CHAPTER 1

### INTRODUCTION AND BACKGROUND

Recent technological developments in nanotechnology provide a multitude of highly desirable products ranging from near 100% efficiency lighting devices [1] to molecular level control of drug delivery for non-invasive cancer therapy [2]. However, widespread application of such nanoscale prototype technologies to macroscale systems (such as a flashlight or the human body) must be preceded by the development of low cost, manufacturing techniques by which they can be produced and assembled in massive quantities. The majority of current “top down” nanomanufacturing techniques rely upon templates which are uniformly patterned with nanoscale features. These templates are typically created by traditional integrated circuit (IC) lithographic techniques which have been scaled down to nanoscopic resolution. These techniques yield very high quality products, but require high vacuum processing equipment and stringent cleanliness standards. Consequently, they suffer from low throughput and high cost. However, it is feasible to use such a substrate as a master template, rapidly replicating its features into second generation templates. Nanoimprint lithography (NIL) is a highly effective and widespread example of such an approach; however, NIL is a lithography process incapable of directly producing a robust final product [3].

Thus, a need currently exists for a cost effective mass production method for producing

large scale durable templates which are patterned with precise nanoscale features. Geometrically complex, high aspect ratio microstructures have been successfully replicated into Zirconium based Bulk Metallic Glasses (BMGs), commercially known as the Vitreloy series of alloys from LiquidMetal Technologies [4], by molding them against patterned Silicon or SiO<sub>2</sub> substrates [5,6,7]. Nanoscopic features of limited aspect ratio have been produced in a Palladium based alloy in a similar fashion [8]. Regardless of the specific alloy, the molding occurs with the BMG alloy suspended in a supercooled liquid state, i.e. above its glass transition temperature,  $T_g$  but below its recrystallization temperature  $T_x$  (see Fig. 1-1). In this temperature range, the material demonstrates Newtonian flow behavior. Components and templates formed in this manner exhibit highly desirable mechanical properties; most notably high strength, stiffness, and elastic strain limit [9].

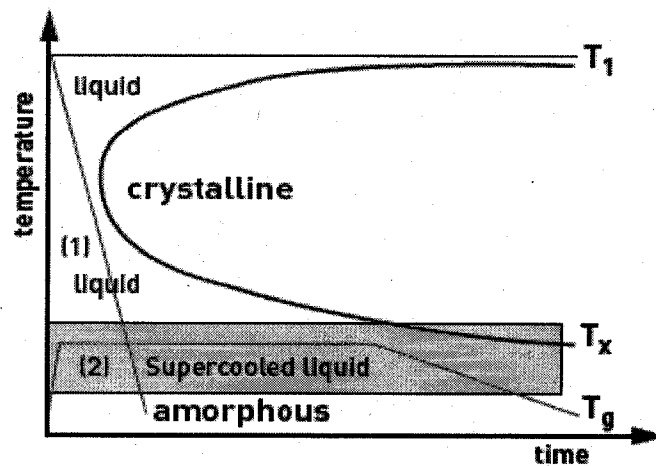


Figure 1-1. Schematic Temperature Time Transition (TTT) diagram illustrating rapid quench casting of a BMG from its molten state (1) and a thermoplastic molding process of the material in its supercooled liquid state (2) [5].

The process of forcing a supercooled BMG alloy into a nanoscopic cavity (typically holes or trenches in Si or SiO<sub>2</sub>) is fundamentally an exercise in highly viscous nanofluidics. Therefore, surface tension based capillary pressure within the BMG may be a critical factor and should be accounted for. Unfortunately, this pressure would oppose the flow of material during the nanoscale molding process if an anti-wetting condition at the BMG/mold interface exists. This condition is exacerbated by the relatively high surface tension typical of BMG alloys [10]. Development of an effective nanoscale molding process for BMG alloys may require efforts to mitigate or reverse this anti-wetting behavior. Kundig et al., have examined the wetting behavior of a molten BMG onto various patterned SiO<sub>2</sub> surfaces at high temperatures (>1200K) and zero applied load, and successfully replicated trench features approximately 30 microns wide by capillary pressure alone [11,12]. This work demonstrates the possibility of not only mitigating capillary pressure resistance, but reversing it entirely such that it aids the molding process.

The specific BMG alloy used in this project is commercially known as Vitreloy-1b (Vit-1b; Zr<sub>44</sub>Ti<sub>11</sub>Cu<sub>10</sub>Ni<sub>10</sub>Be<sub>25</sub>) from LiquidMetal Technologies, Inc. This alloy exhibits a remarkable resistance to crystallization during cooling [13]. This makes the alloy well suited for long duration molding processes which are required to fill complex, high aspect ratio mold features.

In this thesis, the effect of experimentally altering the interfacial interaction between supercooled Vit-1b and the nanoscale mold material is investigated (see Chapter 2). This

was accomplished by performing a series of identical molding experiments using similarly patterned molds of varying chemical composition:  $\text{SiO}_2$ ,  $\text{SiO}_2$  which was coated with Gold, and pure Silicon. Possibly due to interfacial energies, only the Silicon molds produced successfully molded nanoscale features with aspect ratios greater than unity. Furthermore, an analytical model to determine the required molding pressure to overcome the surface tension and initiate flow of the BMG into nanoscale trenches is provided (see Chapter 3). This model was qualitatively validated with the experiments conducted. Finally, the molding process is theoretically analyzed as a squeezed, thin film (see Chapter 4). This provided an estimate of the pressure distribution across the mold.

## CHAPTER 2

### EXPERIMENTAL INVESTIGATION

#### 2.1 Experimental Setup

The first step in investigating the interfacial interaction effect between the BMG and the mold material was to set-up an experimental molding process. Custom fixturing was installed on a model 1350 Instron Mechanical testing machine to allow for precise heating and subsequent rapid quenching of molded specimens to prevent or limit crystallization of the BMG. See Fig. 2-1 for a schematic of the system, and Fig. 2-2 for a picture of the experimental set-up. A similar system was previously employed by Bardt et al. for 3-D microscale molding of Vitreloy 1 [7].

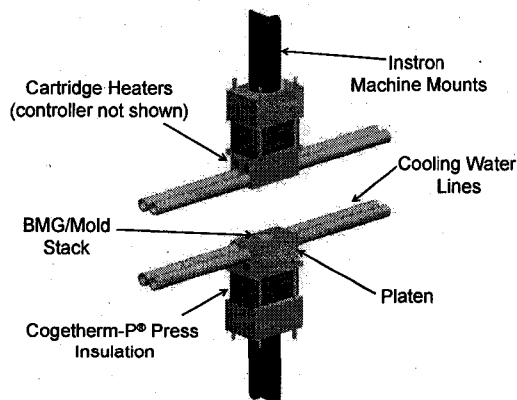


Figure 2-1. Schematic of experimental set-up including components for heating and cooling.

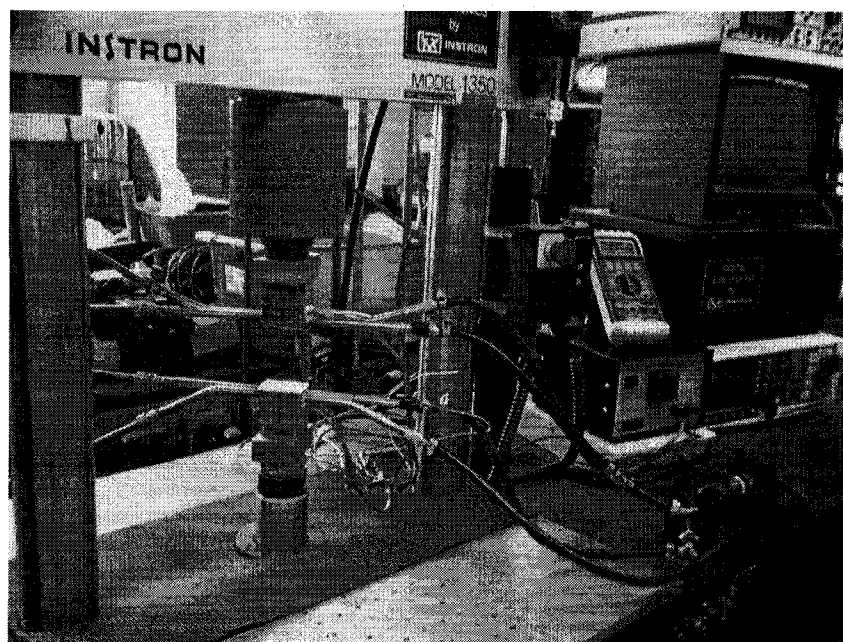


Figure 2-2. Picture of the experimental set-up.

Two identical blocks were machined from C360 brass such that two 100 watt cartridge heaters could be installed in each. (Total system heating power = 400Watts). The heaters are powered by 120V AC current and temperature control is accomplished by an on/off PID Controller Manufactured by Omega Inc (Model CN77333-C2). These heaters were sufficient to heat the system in excess of 500°C, as the brass blocks are thermally isolated from the rest of the system by a high compressive strength insulation (Cogetherm-P) and stainless steel hardware. The BMG must be rapidly quenched while pressure is still being applied in order to assure that material is not allowed to flow back out of the nanoscale mold features. This is accomplished by stainless steel water cooling lines that are installed directly into both brass blocks. In this fashion the system may be quenched from 450°C to 100 in approximately 30 seconds. Commercially pure Nickel platens were



polished to a mirror finish and installed to provide a high temperature, high strength surface that is responsible for applying pressure to the mold chip and BMG.

Brief experimentation with various forming temperatures, and subsequent forming times was conducted, and 450°C for 2 minutes was selected. This temperature is near the middle of the supercooled liquid region for the material, and allows for manageable working times before the onset of recrystallization. Bragg X-Ray Diffraction (XRD) was used to check the formed specimens for recrystallization.

Capillarity and wetting phenomena are integral manifestations of the atomic level attractive forces between the BMG and the mold, which are primarily of the Van Der Waals type [14]. The magnitude of said forces is a function of the dielectric properties of the two materials, i.e. the mold and the BMG [15]. Therefore, molds of three distinctly different compositions were investigated. The first was an insulator, SiO<sub>2</sub>, patterned with trenches ranging in width from 90nm to 340nm. These chips were used as purchased from Philtech Inc. [16]. See Appendix A for details regarding the Philtech Inc. chips. The oxide layer was deposited onto Silicon by Plasma-Enhanced Chemical Vapor Deposition (PECVD), and patterned by X-ray Photolithography. See the left SEM image in Fig. 2-3. The second mold type was created by coating the SiO<sub>2</sub> features of Philtech Inc. chips with approximately 2nm of Titanium (as an adhesion layer) and 15nm of Gold via Ion Beam Assisted Deposition (IBAD). Gold was selected for its chemical inertness and high electrical conductivity. See the right SEM image in Fig. 2-3.

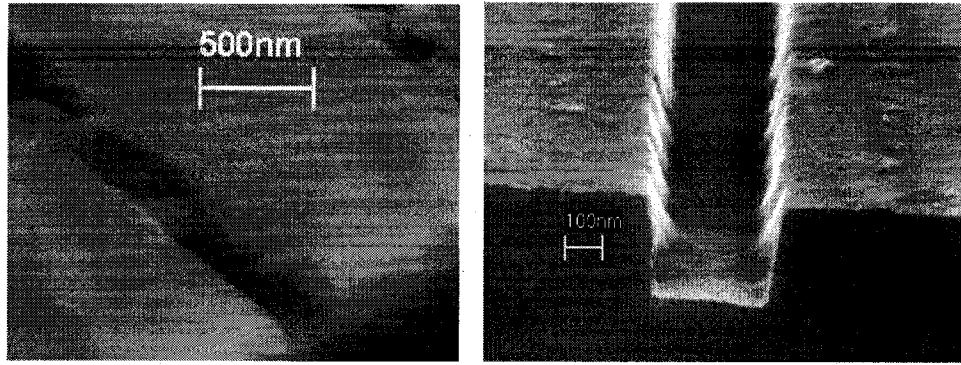


Figure 2-3. (left) Approximately 340nm wide trench in SiO<sub>2</sub> and (right) approximately 300nm wide trench in SiO<sub>2</sub> following Gold deposition.

A third type of mold was custom fabricated with 370nm wide trenches in Silicon chips via Electron Beam Lithography (EBL) and subsequent Reactive Ion Etching (RIE). See SEM image in Fig. 2-4. Trench cross section is slightly tapered because of the anisotropy of the plasma etching process used. Trench depth is approximately 500nm.

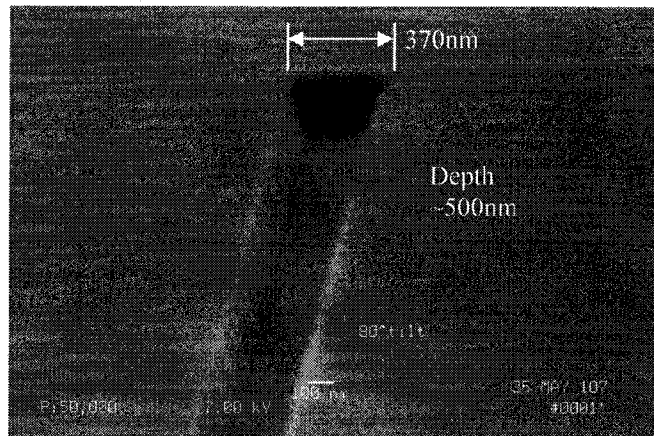


Figure 2-4. A typical trench found in Silicon mold.

BMG plates were provided by LiquidMetal Technologies, and subsequently polished to a mirror finish then diced into billets approximately 4mm x 4mm and approximately 1mm thick. The mirror finish of the billets was found to be a critical parameter.

## **2.2 Experimental Results**

No discernable difference in molding performance was observed between the bare SiO<sub>2</sub> molds and those coated with Gold. Molding experiments were performed with these molds at sequentially higher pressures until fracture of the nanoscale mold features occurred. It was discovered that an applied average molding pressure of 100MPa caused sporadic failure of SiO<sub>2</sub> mold features located near the center of the mold chip, as evident by formed features that were approximately 600nm wide, which is considerably greater than the widest mold feature (340nm). Viscous flow failed to occur in any of these experiments conducted with the SiO<sub>2</sub> or Gold on SiO<sub>2</sub> molds, possibly because capillary pressure could not be overcome prior to mold fracture. The near vertical sidewalls of the molds (Fig. 2-4) were not replicated. Instead the cross sections of the formed features exhibited circular curvature, the radius of which was constant at approximately 400nm, despite considerable variation in trench widths (90-340nm). These low aspect ratio features were characterized with an Atomic Force Microscope (AFM), e.g. see Fig. 2-5. All three of the features shown were formed against 340nm wide trenches in SiO<sub>2</sub>, by BMG at an average pressure of 100MPa. Feature widths greater than 340nm are evidence of localized mold failure (e.g. see area B). Note the consistent radii of curvature despite varying feature widths, e.g. A and B. This same radius was found to be fairly consistent in smaller width features (90 – 340nm) which are adjacent to the area imaged in Fig. 2-5

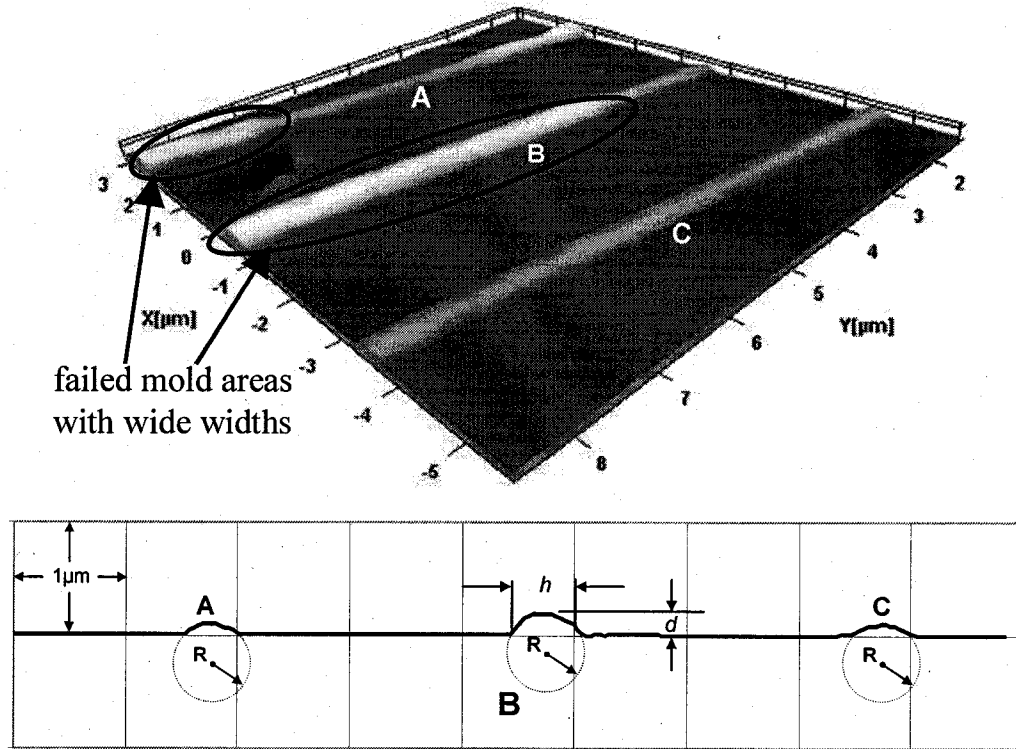


Figure 2-5. AFM image of a Vit-1b specimen formed into a 5mm x 5mm SiO<sub>2</sub> mold at 450°C for 2 minutes with an applied molding pressure of 100 MPa (top) and corresponding cross sectional topography for selected feature cross sections (bottom).

Respective radii of curvatures were then calculated from these sets of height and width values via the following geometric expression

$$R = \frac{1}{2} \left( \frac{h^2}{4d} + d \right) \quad (2-1)$$

where  $R$  is the radius,  $h$  is the width of the feature and  $d$  is the feature height. The resultant radius values are tabulated in Table 2.1

<i>h</i> (nm)	<i>D</i> (nm)	<i>R</i> (nm)
340	95	200
280	60	193
185	31	154
135	14	170
130	13	169
105	7	200
100	7	182
95	6	191

Table 2.1. Geometry values of low aspect ratio features created in SiO<sub>2</sub> mold without viscous flow.

The radii values found were fairly consistent despite the relatively large range of corresponding feature widths. The average radius of curvature of the measured features was found to be 182nm.

The Silicon molds offered considerably better performance under identical processing parameters. Figure 2-6 illustrates features obtained by a molding experiment conducted at 450°C for 2 minutes with an applied average molding pressure of 100MPa using a Silicon mold. In this case the nearly straight sidewalls of the mold features were replicated into patterns centered on the silicon mold chip. The mold trenches were almost completely filled. Note the corresponding taper of the Silicon mold walls in Fig. 2-4. Feature heights were very uniform throughout the 100 micron square patterned area located at the center of the 5mm square mold chip. The heights of these features were measured by AFM to be 470nm tall, resulting in approximately a 1.25:1 aspect ratio.

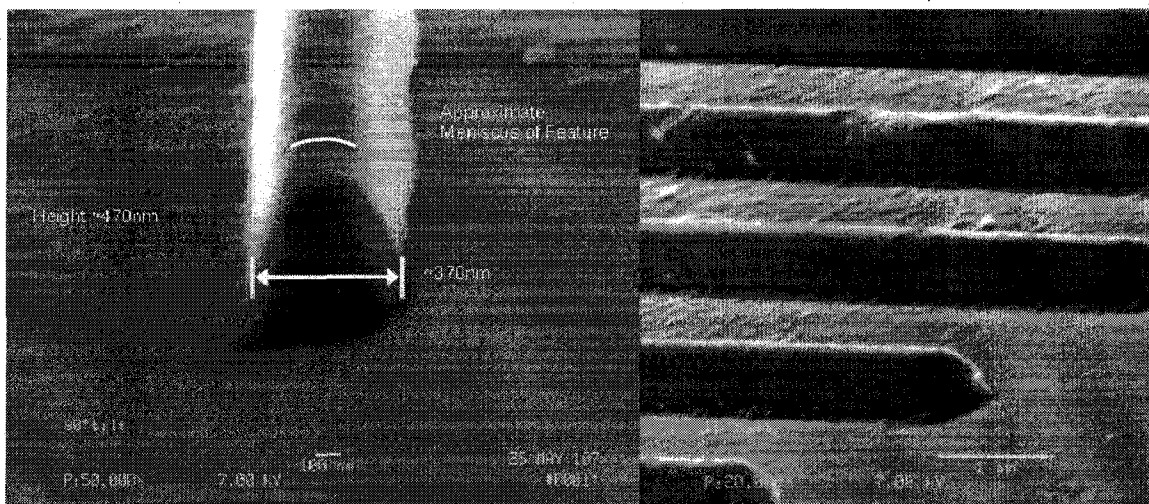


Figure 2-6. SEM image of a Vit-1b specimen formed into a 5mm x 5mm silicon mold at 450°C for 2 minutes with an average applied molding pressure of 100 MPa. (left) Specimen Tilt is 80° providing a near cross sectional view of feature meniscus (right) alternative view demonstrating uniformity of formed features.

### **2.3 Discussion**

It appears that the selection of mold material is a critical processing parameter for this nanoscale molding process. The semiconducting Silicon seemingly exhibited a lesser degree of anti-wetting behavior than the insulating SiO<sub>2</sub> due to interfacial energy considerations. This would be due to the greater magnitude of atomic level attraction between the metallic fluid and semiconducting mold. The alternative explanation is that the molding process did not occur at identical temperatures as intended, which would lead to variations in the viscosity of the BMG and would affect the molding results. Future experiments will control for this parameter more rigorously to determine if this was the possible cause for the molding differences observed.

The intent of Gold coating the SiO<sub>2</sub> molds was to improve molding performance, as Gold is an excellent conductor. However, the 15nm Gold layer was apparently too thin to affect the wetting behavior. Although wetting behavior is an atomic level phenomenon, the electrodynamic forces which constitute it operate over a range of approximately 100nm [15]. Thus, the combined 15nm layer of Gold and 2nm layer of Titanium were too thin to affect the wetting behavior. Similar situations whereby water droplets maintain their anti-wetting behavior atop a plastic substrate which has been coated with a nanoscopic layer of Gold have been documented [14]. Additionally, it is unknown if the Gold layer was able to withstand the shear stresses that would have been induced by the viscous flow of Vit-1b, considering its low yield strength, especially at elevated temperatures.

## CHAPTER 3

### NANO-MOLDING THEORETICAL MODEL

#### 3.1 Model Development

In order to calculate the required pressure to cause viscous flow of the BMG into nanoscale features and the subsequent achievable feature height (see Fig. 3-1), a nano-molding theoretical model was developed. This model is based on a force equilibrium approach. First, assumptions for the model must be validated. Because of the nanoscopic size of mold features into which the BMG is flowing, the continuum assumption of fluid mechanics must be validated by computation of the Knudsen number for the viscous flow during molding,  $Kn$ , a dimensionless ratio of molecular mean free path,  $\lambda$  to the width of the mold channel,  $h$ .

$$Kn = \frac{\lambda}{h} \quad (3-1)$$

For the case of a condensed liquid (molten metal),  $\lambda$  may be taken as the atomic diameter of Zirconium, the largest and most prevalent of the constituent elements of Vit 1b, approximately 310 pm. Therefore, despite the nanoscopic width of the mold features (100-370nm), characteristic  $Kn$  values are the order of  $10^{-3}$ , supporting the use of the



continuum assumption. The Knudsen number would need to be near or above unity for the continuum mechanics assumption to be invalid.

Other effects within the physical system which need to be assessed are inertial effects within the flowing BMG and the compression of air in the mold cavities. Reynolds number values for the molding process are assumed to be within the creeping flow regime because of the extremely high viscosity of supercooled Vit-1b (approximately  $2 \times 10^7$  Pa-s at 450°C) [10]. Thorough verification of this assumption requires an expression for flow velocity during the molding process, which will be derived as part of the model. Therefore validation will be performed at the end of this section. In the mean time, inertial effects will be neglected.

The pressure induced by compressing the air in the mold features must also be accounted for, but once again matters are complicated by the nanoscopic size of the mold features, which are initially filled with air. In this case,  $\lambda$  of Eq. 3-1 is taken as the mean free path of gas molecules (not the molecular diameter), and this value is typically on the order of 100nm. Resulting values of the Knudsen number are often greater than unity and do not support the use of the Ideal Gas Law (a continuum assumption) for most nanoscopic gas flows. This is because the Ideal Gas Law is essentially an equation of state which idealizes a gas as a continuum, and the Van Der Waals Equation of state is essentially a modified version of the Ideal Gas Law which accounts for the size of the molecules in the gas, and their attractive properties to each other. However, in this specific instance, the Ideal Gas Law is known to uniformly overestimate the pressure increase on account of a

constant temperature compression, and can be used to generate an upper bound estimate which is adequate in this case.

$$PV = nRT \quad (3-2)$$

where  $P$  is pressure,  $V$  is volume,  $n$  is the number of moles of gas,  $R$  is the Universal Gas Constant, and  $T$  is temperature. For a constant mass, constant temperature compression Eq. (3-2) dictates that a given percentage decrease in volume results in an inversely proportional percentage increase in pressure. For instance, if the air in a given mold channel is compressed to one tenth of its original volume (i.e. 90% of the mold cavity is filled), it will undergo a ten fold increase in pressure. Taking atmospheric pressure to be 100 kPa (i.e. the initial air pressure in the mold prior to the process), the pressure within this compressed gas will be approximately 1 MPa which is much less than typical molding pressures (e.g. 100-150MPa). The actual pressure of the air compressed in the nanoscopic mold features is expected to be even lower than this value.

The remaining viscous ( $\mu$ ) and capillary ( $\gamma$ ) pressures which must be overcome to accomplish molding are modeled as separate terms, and equated to the applied molding pressure in order to satisfy equilibrium. It is assumed that these terms may be linearly superimposed. This concept was first proposed by Schroers [5].

$$P_{BMG} = P_{\mu} + P_{\gamma} \quad (3-3)$$

where  $P_{BMG}$  is the total applied molding pressure,  $P_{\mu}$  is the viscous pressure term, and  $P_{\gamma}$  is the capillary pressure term. Note that a frictionless condition is assumed for the flow, and therefore a pressure term to account for the frictional effect between the advancing flow and the mold feature is neglected.

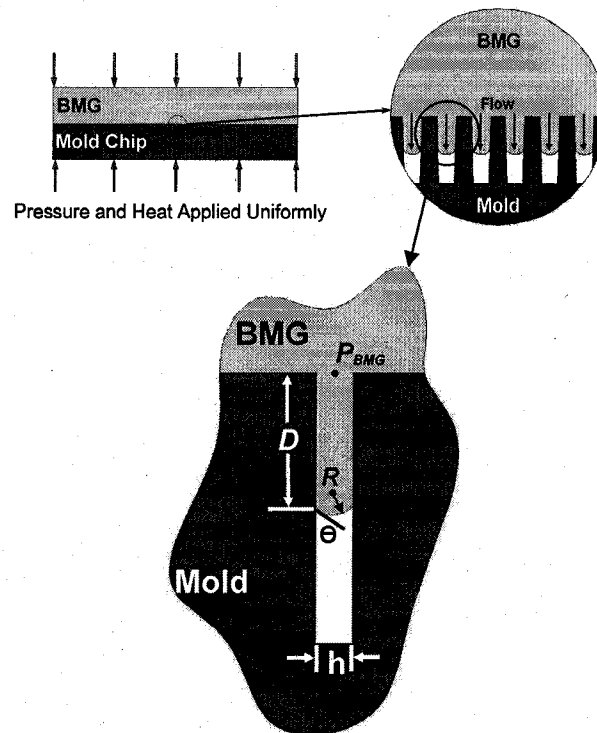


Figure 3-1: Schematic of molding process including definitions of parameters.

The capillary pressure is calculated for a worst case, completely anti-wetting condition between the BMG and mold trench (i.e.  $\theta=0$  in Fig. 3-1). This results in a semicircular meniscus at the tip of the advancing mold feature of radius,  $R$  equal to one half of the mold trench width,  $h$ .

$$P_r = \frac{\gamma}{R} = \frac{2\gamma}{h} \quad (3-4)$$

where  $\gamma$  is the surface tension of the BMG. The surface tension of Vit-1b at temperatures below its liquidus temperature is not currently documented. Mukherjee et al. measured and documented the surface tension of this material at temperatures ranging from its melting point of 720°C to 1030°C, and observed a near constant value of approximately 1.5 N/m over this range. This lack of temperature dependence is atypical of molten metals, which usually exhibit a linear decrease in surface tension as temperature is increased [10]. In order to determine this parameter for our model, it was deduced from the geometry of features formed against SiO<sub>2</sub> where it is apparent from their shape that no viscous flow occurred as they were being formed ( $P_\mu=0$ ). Eq. (3-3) may then be re-written as

$$P_{BMG} = P_\gamma \quad (3-5)$$

and the local pressure in the BMG is therefore set equal to the capillary pressure within the formed feature. The magnitude of the surface tension of Vit-1b at 450°C may then be deduced by rearranging Eq. (3-4) yields

$$\gamma = P_{BMG} R \quad (3-6)$$

This equation was then used to calculate a surface tension value of 27 N/m using the average radius of curvature (182nm) previously documented from values in Table 2.1,

and the known pressure within the BMG. Although the accuracy of this method is severely limited, the resulting value is a reasonable approximation. Note however that this value is much higher than typical metals.

Pressure loss due to viscous dissipation is modeled as a modified version of the pressure drop experienced in viscous Poiseuille flow. Modification is required to account for the fact that the flow depth,  $D$ , varies with time,  $t$ , as the BMG fills the initially empty mold feature. In this sense this model is fundamentally different than that proposed by Schroers et al. [5,6].

$$P_{\mu} = \frac{12\mu}{h^2} D(t) \frac{dD(t)}{dt} \quad (3-7)$$

where  $\mu$  is the viscosity of the BMG.

Solving this differential equation yields the following parabolic expression for final molded feature depth as a function of time.

$$D(t) = h \sqrt{\frac{P_{\mu}}{6\mu} t} \quad (3-8)$$

The instant  $t=0$  is defined at the onset of viscous flow, which cannot occur until  $P_{\gamma}$  overcome by the applied molding pressure. Although molding temperature,  $T$ , is not included explicitly in this expression, it is a critical processing parameter. The viscosity

of Vit-1b decreases drastically as temperature is increased, allowing the material to flow much easier at higher temperatures [10]. However, the choice of molding temperature also defines the maximum allowable processing time, because BMGs are metastable by nature, and gradually crystallize when heated above their glass transition temperature (400°C for Vit-1b) [13]. Higher temperatures result in faster recrystallization (see Fig. 1-1). Complete recrystallization of the material is detrimental to its nanoscale homogeneity and bulk mechanical properties and thus should be avoided. The effect of temperature on the viscosity and recrystallization time of Vit-1b has been clearly documented by Schroers et al [6].

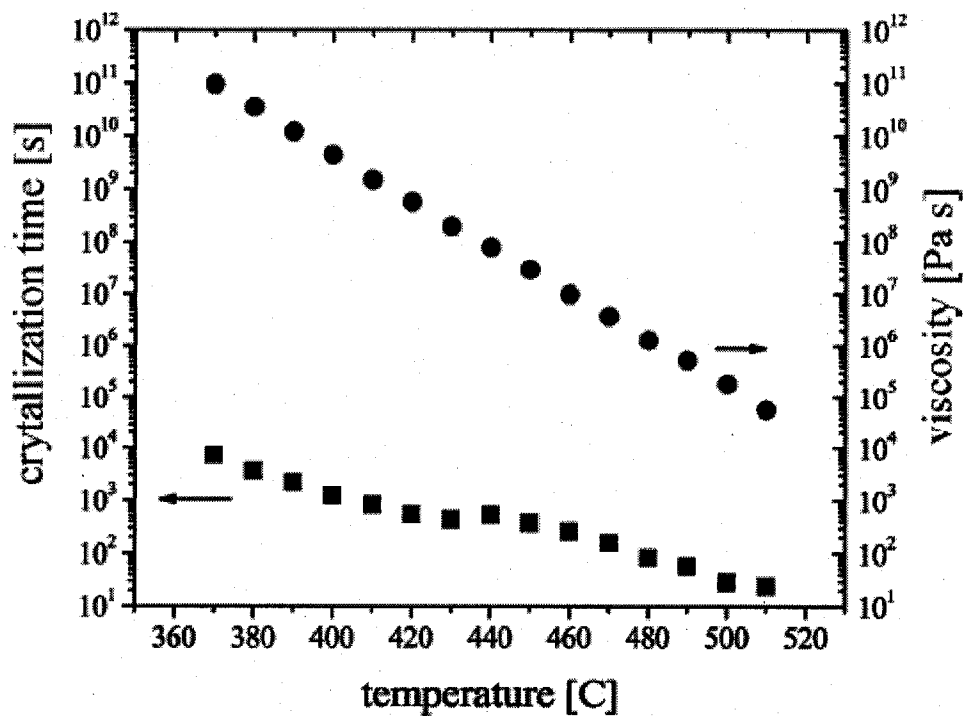


Figure 3-2. Recrystallization time and viscosity vs temperature for Vit-1b as documented by Schroers et al [6].

Finally, in order to validate the creeping flow assumption of Eq. 3-7, the Reynolds number,  $Re$  must be calculated for the molding process.

$$Re = \frac{dD}{dt} \frac{h\rho}{\mu} \quad (3-9)$$

where  $\rho$  is the mass density of the BMG (6100 kg/m<sup>3</sup>).

Rearranging Eq. (3-7) yields an expression for flow velocity

$$\frac{dD}{dt} = \frac{P_{\mu} h^2}{12 \mu D(t)} \quad (3-10)$$

Substitution of Eq. (3-10) into Eq. (3-9) yields

$$Re = \frac{P_{\mu} h^3 \rho}{12 \mu^2 D(t)} \quad (3-11)$$

It is known that the flowrate will be greatest at the instant immediately following the onset of viscous flow ( $t=0+$ ), thus a reliable upper bound estimate for the maximum flowrate (and subsequent Reynolds number) may be obtained at an instant in time directly after viscous flow has initiated by setting  $D(t)$  equal to 1nm and the pressure dissipated,  $P_{\mu}$ , equal to 1 Pa. Additionally,  $h$  is set equal to 500nm and  $\mu$  is known to be

equal to  $2 \times 10^7$  Pas for Vit-1b at the typical molding temperature of  $450^\circ\text{C}$ . The resultant Reynolds Number is  $6.35 \times 10^{-9}$ , strongly supporting the creeping flow assumption.

### **3.2 Results**

The relationship between applied molding pressure and expected feature height based on Eqs. (3-3), (3-4) and (3-8) for two temperatures and feature widths is presented in Fig. 3-3. Molding times have been set equal to 10% of the temperature dependent, isothermal, zero strain rate values, at which crystallization occurs [6]. As Fig. 3-3 illustrates, higher molding temperatures are predicted to yield better results, despite the required reduction in molding time before the BMG would crystallize. Note however that the  $\gamma$  may well be temperature dependent, and the value deduced from the  $450^\circ\text{C}$  experimental investigations ( $27\text{N/m}$ ) has been used for the  $420^\circ\text{C}$  cases as well. Note that the filled depth,  $D$ , as shown in Fig. 3-1 is from the top of the mold trench to the location where the BMG and mold contact, i.e. not the apex of the radius portion of the BMG. This is why the filled depth in Fig. 3-3 is zero until the pressure is sufficient to overcome the capillary pressure.



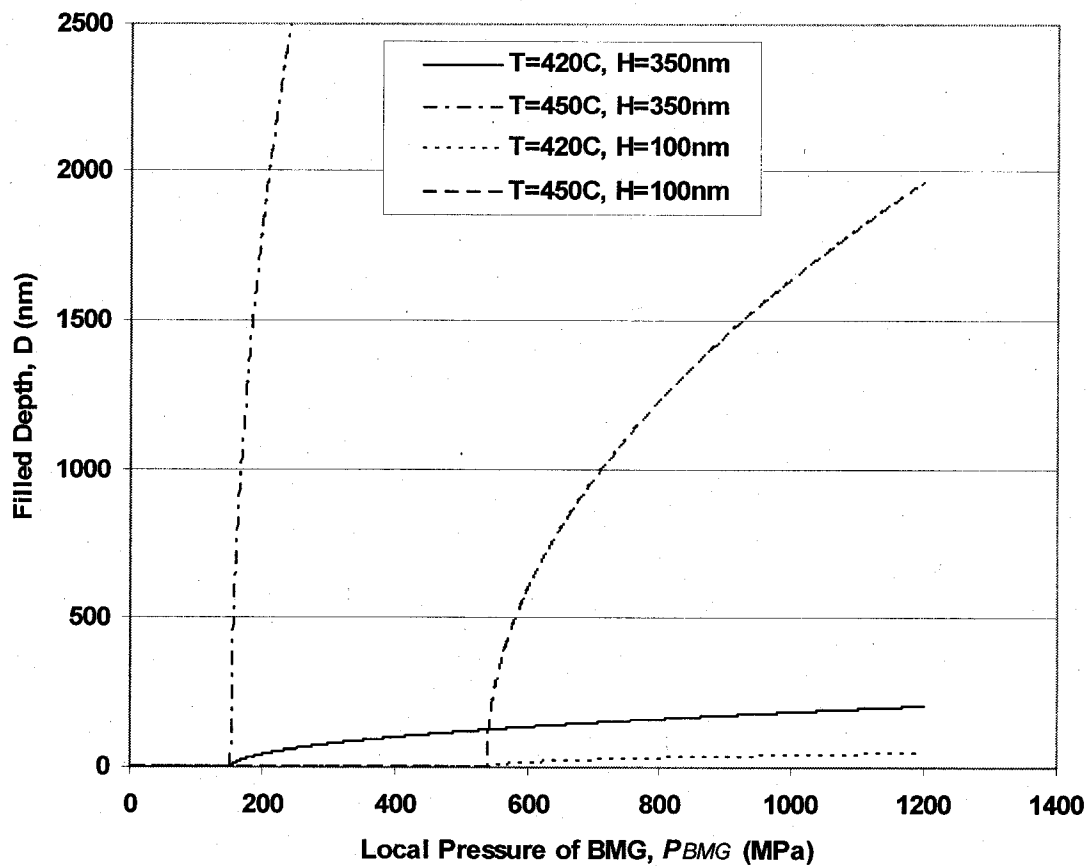


Figure 3-3: Predicted filled depth for two mold trench widths and molding temperatures versus applied pressure.

### 3.3 Discussion

When comparing Figs. 2-5 and 2-6, a reduction in capillary pressure from the completely anti-wetting condition possibly occurred based on the meniscus of the features formed into a silicon mold (Fig 2-6). The radius of curvature of this feature is considerably greater than the width of the top of the feature, indicating that the contact angle,  $\theta$ , between the BMG and the mold (see Fig. 3-1) was greater than zero and therefore

completely anti-wetting behavior did not occur. This observation is in good qualitative agreement with the proposed model. Validation of the viscous portion of this model is currently not possible due to the limited depth of the features on the molds which are currently available.

Based on this model, higher temperatures with short molding times should be used in future experiments to increase feature heights. The  $\gamma$  value for temperatures other than 450°C will need to be deduced in a similar fashion to provide accurate model results. Furthermore, modifications to Eq. (3-4) to reduce the completely anti-wetting assumption are required to allow more accurate calculations of feature heights for molding systems which do not exhibit completely anti-wetting behavior.

## CHAPTER 4

### SQUEEZED THIN FILM THEORETICAL MODEL

#### 4.1 Model Development

It is the pressure within the BMG that is directly responsible for driving the nanomolding process (not to be confused with the constant pressure applied to the mold chip). Therefore an understanding of the pressure distribution across the BMG during the molding process is essential. In a macroscopic sense, the molding process can be modeled well as a squeezed viscous thin film since the supercooled liquid BMG is known to behave as an incompressible, Newtonian fluid at elevated temperatures. This approach is typically employed when the film thickness is much smaller than the film width, which is true in this case (i.e. a mold of 5 mm x 5 mm with an initial BMG thickness of approximately 1 mm which rapidly decreases as the molding process progresses). Such a model neglects the small variation in pressure across the thickness of the film. Additionally, although the flow is not at a steady state, inertial effects within the flowing film are also neglected by a creeping flow assumption, which is supported by the very low characteristic Reynolds Number of the flow which has been calculated at the end of this section. This Reynolds Number calculation is performed for the macroscopic flow of material as a thin film, not to be confused with the calculation performed in Chapter 3 for the nanoscopic flow of material into the mold features.

A typical molding process consists of three distinct phases. First the film is heated to a constant temperature (e.g. 450°C) by contact with the heated platens (Fig. 4-1a.). It is then squeezed by a constant force applied equally by the upper platen and the nanopatterned molding chip (Fig.4-1b.). Finally, once the molding process is completed, the film is rapidly quenched back to room temperature and the applied pressure is removed (Fig. 4-1c.). The process produces a thin film of BMG between the mold and the platen.

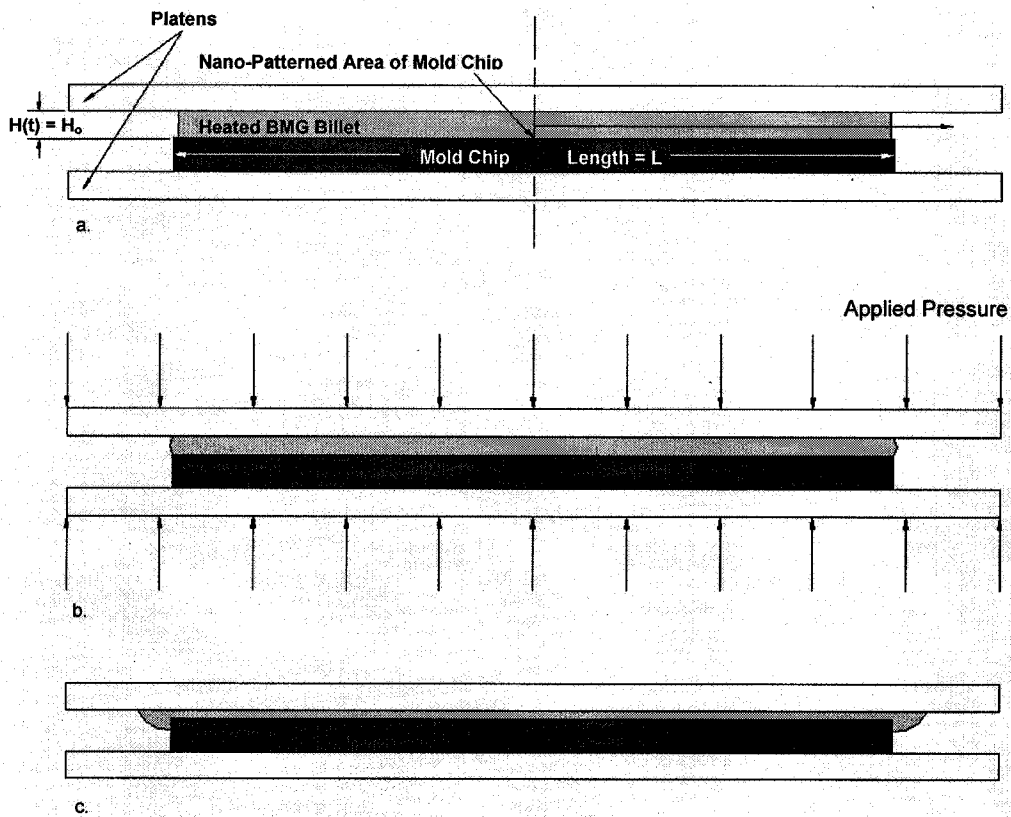


Figure 4-1. Macroscopic schematic of the molding process a) initially, b) as the BMG is squeezed and flows laterally, and c) with the final thin film of BMG between the mold and the platen.

The equations for the squeezed, thin film model follow. Simplification of the Navier-Stokes equations and the continuity condition for a squeezed viscous film yields the following expression

$$\frac{1}{\mu} \frac{d}{dx} \left( H^3 \frac{dp}{dx} \right) = -12 \frac{dH}{dt} \quad (4-1)$$

where  $\mu$  is the viscosity,  $x$  is the lateral distance from the center of the mold,  $H$  is the film thickness (see Fig. 4-1), and  $p$  is the local pressure within the thin film. This equation is commonly known as the Reynolds Equation for a squeezed film [17]. Taking advantage of symmetry, this expression is integrated from the center of the mold ( $x=0$ ) to the edge of the squeezed film ( $x=L/2$ , where  $L$  is the total width of the mold). This yields the following expression for the lateral pressure gradient in the film of BMG.

$$\frac{dp}{dx} = -\frac{12\mu}{H^3} \frac{dH}{dt} x \quad (4-2)$$

where the constant of integration is found to be zero by applying the symmetry boundary condition at the center of the chip

$$\left. \frac{dp}{dx} \right|_{x=0} = 0 \quad (4-3)$$

Integrating a second time and applying the free surface condition at the edge of the chip

$$p(L/2) = 0 \quad (4-4)$$

yields the following expression [17]

$$p_{BMG}(x,t) = -\frac{6\mu}{H(t)^3} \frac{dH}{dt} (4x^2 - L^2) \quad (4-5)$$

Thus, the pressure distribution in the film is now defined as a function of position and time. However, this expression is not directly useful, as the film thickness function is still undefined. It is therefore necessary to equate the average applied pressure with the undefined film pressure as depicted in Fig. 4-2.

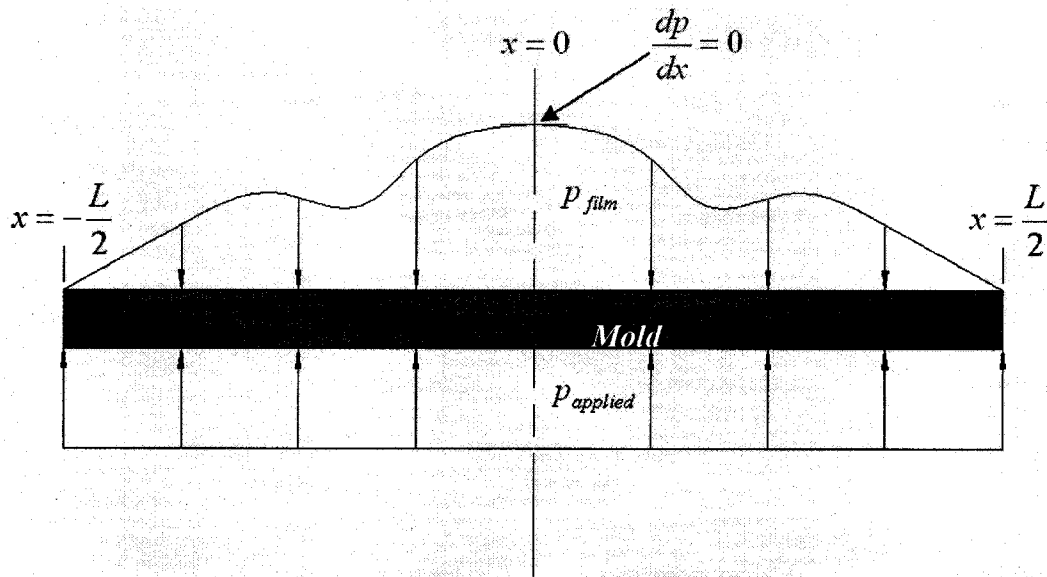


Figure 4-2. Equating of average applied pressure with undefined film pressure.

Neglecting inertial effects and once again taking advantage of symmetry, this condition may be expressed as

$$\int_0^{L/2} P_{\text{applied}} dx = \int_0^{L/2} P_{\text{BMG}} dx \quad (4-6)$$

where the film pressure is defined by Eq. (4-5) and the applied molding pressure is known to be constant with respect to time and location on the surface of the mold chip

$$P_{\text{applied}} = \frac{F}{A} = \frac{F}{L^2} \quad (4-7)$$

where the mold chip is square with a dimension of  $L$ . Therefore Eq. (4-6) becomes

$$\int_0^{L/2} \frac{F}{L^2} dx = \int_0^{L/2} \frac{6\mu}{H(t)^3} \frac{dH}{dt} (4x^2 - L^2) dx \quad (4-8)$$

Performing this integration and rearranging yields the desired expression for the thinning rate of the squeezed film, as a function of the film viscosity and known molding system parameters

$$\frac{dH}{dt} = -\frac{F}{2L^4 \mu} H(t)^3 \quad (4-9)$$

Upon examination of this expression it is observed that the rate of film thinning *decreases* at a rate which is proportional to a reduction in film thickness cubed. Recall, that Eq. (4-5) states that the pressure within the film will *increase* at a rate which is proportional to a reduction in film thickness cubed. Therefore, substitution of Eq. (4-9) into Eq. (4-5) results in a cancellation of the effect of the thinning film thickness. Subsequently, all time dependence of the pressure within the thin film of BMG is removed, since the film thickness was the only time dependent parameter in Eq. (4-5). For similar reasons, the effect of material viscosity also cancels out of the following expression.

$$p(x)|_{film} = -\frac{3F}{2L^2} \left[ \left( \frac{2x}{L} \right)^2 - 1 \right] \quad (4-10)$$

Finally, recognizing the applied molding pressure term in the above expression allows the equation to be re-written as

$$p(x)|_{film} = -\frac{3}{2} P_{applied} \left[ \left( \frac{2x}{L} \right)^2 - 1 \right] \quad (4-11)$$

This expression allows for the determination of the local pressure within the squeezed film of BMG as a function of the known applied molding pressure. A properly scaled representation of the squeezed, thin film pressure distribution is provided in Fig. 4-3.



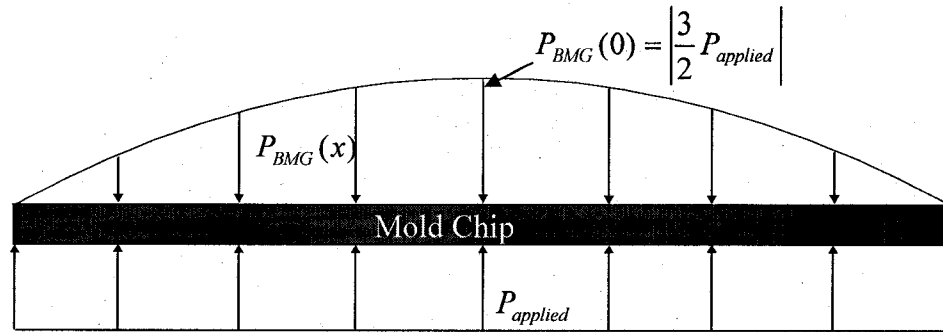


Figure 4-3. Predicted pressure distribution within the thin film of BMG

Finally, the creeping flow assumption of the thin film model can be verified by calculation of the Reynolds Number, which is defined as

$$Re = \frac{UH\rho}{\mu} \quad (4-12)$$

where  $\rho$  is the mass density of the BMG and  $U$  is the lateral mean flow velocity of BMG, which may be calculated by conservation of mass and incompressibility (Fig 4-4 and Eq. (4-13)).

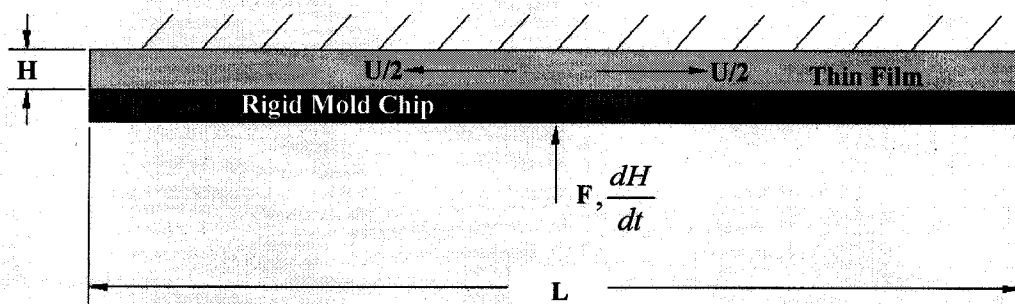


Figure 4-4. Schematic of material flow in the molding process.

$$\frac{U}{H} = \frac{dH/dt}{L} \quad (4-13)$$

Substitution of Eq. (4-13) into Eq. (4-12) allows the Reynolds number to be expressed as

$$\text{Re} = \frac{H^2 \rho}{\mu L} \frac{dH}{dt} \quad (4-14)$$

and substitution of Eq. (4-9) into this expression yields

$$\text{Re} = \frac{H^5 \rho F}{4\mu^2 L^3} \quad (4-15)$$

Application of typical molding parameters (e.g.  $\mu$  equal to  $2 \times 10^7$  Pa/s,  $\rho$  equal to  $6100$  kg/m<sup>3</sup>,  $L$  equal to  $5$  mm,  $H$  equal to  $1$  mm,  $F$  equal to  $2000$  N) to Eq. (4-15) results in a characteristic Reynolds number equal to  $2.44 \times 10^{-12}$  which strongly supports the creeping flow assumption..

Unfortunately, the limited aspect ratios of the mold features available to date (Fig. 2-4) are inadequate for validation of these calculations. Efforts are currently underway to fabricate a series of high aspect ratio molds from silicon via Deep Reactive Ion Etching (DRIE). Experimentation with these molds will allow for direct validation of both the thin film and nanofluidic molding models.

## CHAPTER 5

### CONCLUSIONS

Drastically better molding performance was observed for the Silicon (semiconductor) molds in comparison with those patterned in SiO<sub>2</sub> (insulator), under identical molding parameters. This difference in performance may be due to the difference in wettability between the two mold materials and a resulting difference in capillary pressures during the molding process. The deposition of Gold (conductor) upon bulk SiO<sub>2</sub> molds failed to impact molding performance, presumably because the deposited layer was too thin. A surface tension value of 27N/m was deduced from the curvatures of formed features for Vitreloy-1b at 450°C. Note that this value is much higher than typical metals. The molding pressure required to initiate flow was found to be in qualitative agreement with the proposed theoretical model for the molding process. Additionally, a thin film model was proposed in order to calculate the local pressure within the BMG as a function of the pressure applied to the mold chip by the forming system. Complete validation of both the thin film and the nanomolding model are not currently possible on account of the limited aspect ratio of available mold chips.

## CHAPTER 6

### FUTURE WORK

As previously stated, the primary impediment to further progress is the availability of molds which possess high aspect ratio nanofeatures. In order to fulfill this demand a nanofabrication process has been developed by which a 3" silicon wafer will be patterned at the Kostas Center for Nanofabrication at Northeastern University, and subsequently shipped to a third party (MemsExchange [19]), for Deep Reactive Ion Etching. This wafer will contain two distinctly different mold patterns, the first of which will serve as a general nanomolding test bed. It will measure 5mm x 5mm and contain trenches ranging in width from 50nm to 300nm, and holes with diameters of 50nm and 100nm. This mold pattern also contains a 100 $\mu$ m long wedge which narrows from 3 microns to a sharp point which will serve as a variable width trench and allow for direct study of capillary effects. The chip layout and pattern detail of this chip is presented in Fig. 6-1.

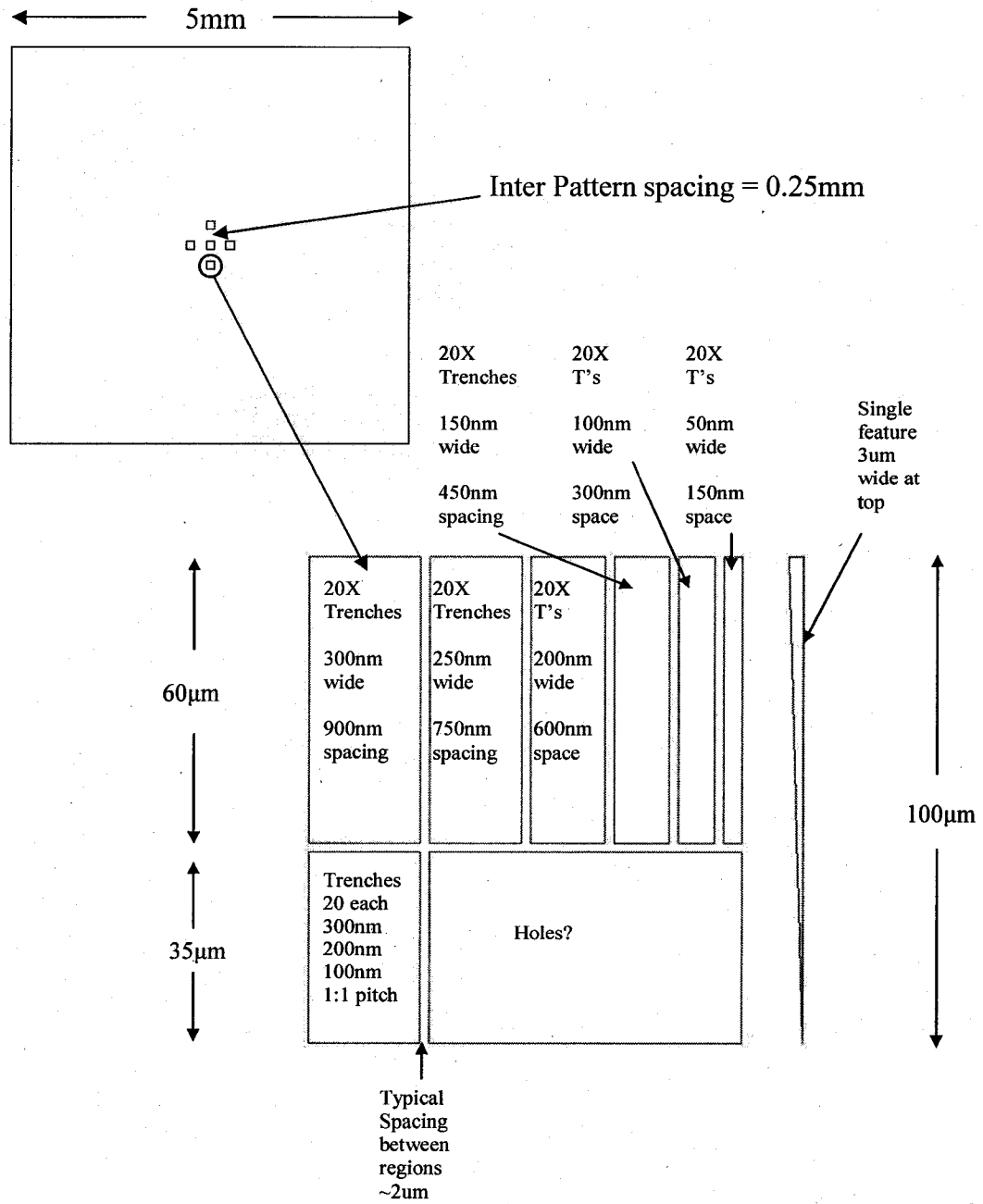


Figure 6-1. Chip pattern layout (top) and pattern detail (bottom) of nanomolding test chip to be fabricated via Deep Reactive Ion Etching.

The second mold type will serve to directly validate the thin film model. It will be considerably wider (10mm x 10mm) to offer good horizontal resolution between an array of identical, orthogonally oriented patterns which consist of 300nm and 200nm trenches. A schematic of this mold chip is provided as figure 6-2.

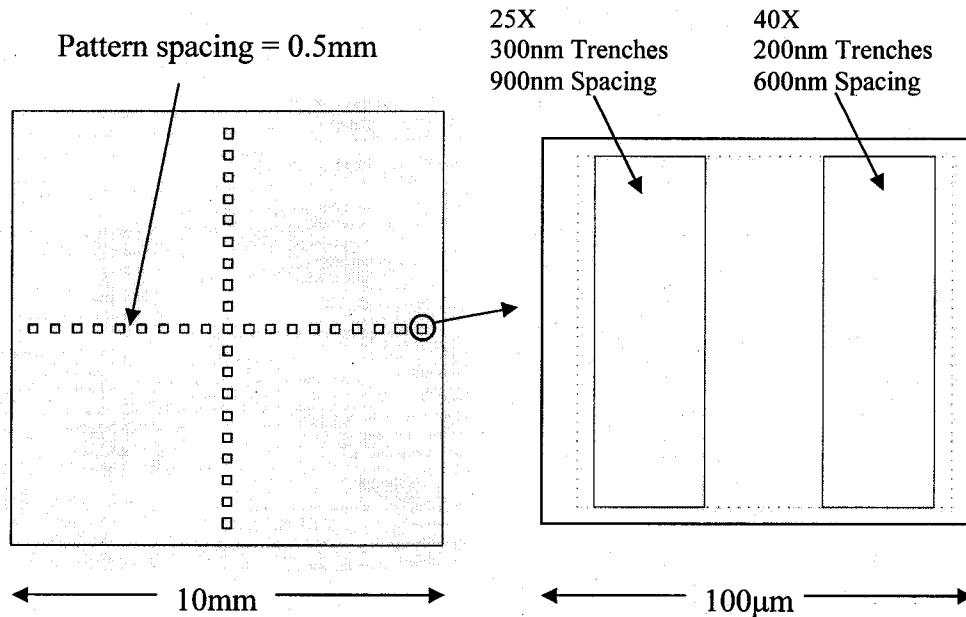


Figure 6-2. Pattern layout (left) and pattern detail (right) for chips intended for verification of thin film model

Once these high aspect ratio molds are obtained, more extensive testing will be possible. Specifically, a series of mold chips fabricated per Fig. (6-1) could selectively be doped using spin on diffusion layers of Phosphorus (n-type dopant) and Boron (p-type dopant). Preliminary experimentation with doping silicon substrates by thermal diffusion has already begun and once this process is completed it will be possible to selectively control the dielectric properties of geometrically identical silicon molds, and study the effect of

this parameter with respect to molding performance. Through this approach it may be possible to reverse the anti wetting behavior exhibited between the BMG and mold, flipping the direction of the capillary pressure such that it aids the molding process. This will allow for the use of considerably lower molding pressures and higher aspect mold features to be fabricated in BMG substrates.

Finally, work must be conducted with respect to mold durability. Currently, Silicon molds are sacrificial as they are severely damaged during quenching and/or separation from the formed BMG substrate. In order for this nanoscale molding process to become a true mass production process, the mold should be reusable. Reusable molds fabricated by ion milling various metallic thin films (Titanium, Nickel and Chromium) or Sapphire wafers ( $\text{AlO}_3$ ), alternatively carefully designed mold release layers could be developed and applied to silicon molds

## REFERENCES

1. Williams, E., Haavisto, K., Li, J. and Jabbour, G. "Excimer-based white phosphorescent organic light emitting diodes with nearly 100 % internal quantum efficiency" *Advanced Materials*, v 19, n 2, Jan 20, 2007, p 197-202.
2. Subramani, K. Applications of nanotechnology in drug delivery systems for the treatment of cancer and diabetes. Source: *International Journal of Nanotechnology*, v 3, n 4, 2006, 557-80.
3. Chou, S., Krauss, P. and Renstrom, J., "Nanoimprint Lithography" *Journal of Vacuum Science Technology B*, Nov/Dec 1996 pp. 4129-4133.
4. LiquidMetal Technologies, Inc., [www.liquidmetal.com](http://www.liquidmetal.com)
5. Schroers, J. "The Superplastic Forming of Bulk Metallic Glasses", *Journal of Metals*, May 2005, pp. 35-9
6. Schroers, J., Pham, Q., Desai, A., "Thermoplastic Forming of Bulk Metallic Glass-A Technology for MEMS and Microstructure Fabrication", *Journal of Microelectromechanical Systems*, v16 N 2, April 2007 pp. 240-7.
7. Bardt, J.A., Ziegert, J.C., Schmitz, T., Sawyer, W.G., and Bourne, G., "Precision Molding of Complex Metallic Micro-structures", *Proceedings of the International Conference on Micromanufacturing – ICOMM*, Urbana-Champaign, IL, Sept. 13-15, 2006, pp. 274-279.
8. Saotome, Y., Itoh, K., Zhang, T. and Inoue, A. "Superplastic Nanoforming of Pd-Based Amorphous Alloy," *Scripta Materialia*. 44, 2001, pp. 1541–1545.



9. Johnson, W. L. and Samwer K., "A Universal Criterion for Plastic Yielding of Metallic Glasses with a  $T = T_g + 2/3$  Temperature Dependence", *Physical Review Letters*, 4 Nov 2005, 195501.
10. Mukherjee, Johnson W., and Rhim, W. "Non-contact Measurement of High-Temperature Surface Tension and Viscosity of Bulk Metallic Glass-Forming Alloys Using the Drop Oscillation Technique", *Applied Physics Letters* 2005 86, 014104.
11. Kundig, A. Dommann, W.L. Johnson and P.J. Uggowitzer, "High Aspect Ratio Micro Mechanical Structures Made of Bulk Metallic Glass", *Material Science and Engineering A*, 2004, pp. 327-331.
12. Kundig, A. Dommann, W.L. Johnson and P.J. Uggowitzer, "High Aspect Ratio Micro Mechanical Structures Made of Bulk Metallic Glass", *Material Science and Engineering A*, 2004, pp. 327-331.
13. Waniuk, T. Schroers, J. and Johnson, W.L. "Timescales of crystallization and viscous flow of the bulk glass-forming Zr-Ti-Ni-Cu-Be alloys" *Physical Review B* 67, 2003 184203.
14. De Gennes, P., Brochard, R. and Quere D. *Capillarity and Wetting Phenomena*, Springer 2004
15. Parsegian, V. *Van Der Waals Forces, A Handbook for Biologists, Chemists, Engineers and Physicists*, Cambridge 2006
16. Philtech Inc., [www.Philtech.co.jp](http://www.Philtech.co.jp)
17. R. Panton, *Incompressible Flow*, Wiley-Interscience 1984.
18. Waniuk, T. Schroers, J. and Johnson, W.L. "Critical cooling rate and thermal stability of Zr-Ti-Cu-Ni-Be alloys" *Applied Physics Letters* v78, 9 Feb 2001 pp 1213-5

19. [www.memsexchange.org](http://www.memsexchange.org)

20. Rason, K., Kinsey, B., "Nanoscale Molding of a Zirconium based Bulk Metallic Glass" *Proceedings of IMECE 2007: ASME International Mechanical Engineering Conference and Exposition* Seattle, WA Nov 11-15, 2007.